The Effect of Inter-Fiber Distance on the Interfacial Properties in E-glass Fiber/Epoxy Model Composites

C. K. Moon,[1] G. A. Holmes,[2] W. G. McDonough[2]

[1]Division of Materials Science and Engineering, Pukyong National University, Yong dang-Dong, Nam-Gu, Pusan 608-737, South Korea
[2]Polymer Division, National Institute of Standard and Technology, Gaithersburg, Maryland 20899-5843

ABSTRACT: The effect of interfiber distance on the interfacial properties in E-glass fiber/epoxy resin composites has been investigated using one and two fiber with various interfiber distance fragmentation test specimens. In addition, the effect of the fiber surface treatment on the interfacial properties has been studied. As a result, we found that the interfacial shear strength increased with the increasing of interfiber distances from 0 to 50 μm and then the ones were saturated regardless of sized and unsized fibers. It was seen that the interfacial shear strengths saturated were in close agreement with those of the single fiber fragmentation tests. We also found that when the interfiber distance was very small, the stress distribution pattern was shown like one fiber, and when the interfiber distance was greater than 50μm, the stress distribution pattern was independent on between fibers. Finally, the interfacial shear strength evaluated using two E-glass fiber/epoxy resin fragmentation test method is shown as real values in-site regardless of the fiber surface treatment and interfiber distance. © 2007 Wiley Periodicals, Inc. J Appl Polym Sci 105: 3483–3491, 2007

Key words: interfiber distance; interfacial properties; fragmentation test; matrix crack; damage

INTRODUCTION

The properties of the interphase region between reinforcing fibers and polymer matrixes play a very important role in influencing the mechanical properties and final performance (e.g., strength, failure behavior) of composites. One of the most critical and fundamental properties for evaluating the mechanical response and durability of this region, and hence the composite, is the interfacial shear strength (IFSS).[1]

The interphase region transfers the stress from the matrix to the reinforcing fibers and therefore affects a composite's strength and failure behavior. The transfer rate of the stress is related to the IFSS. If the IFSS is too low (i.e., low transfer rate), fiber failure initiates extensive debonding along the length of the fiber. Debonding reduces the effectiveness of the reinforcing fiber and the composite's strength. In addition, weak bonding between the interphase region and the reinforcing fiber lowers the transverse strength of the composite and reduces the resistance of the composite to environmental conditions. Interestingly, it has been suggested that a composite's fracture toughness may be improved by a proper IFSS.[2,3]

Interphase properties are generally improved by the use of coupling agents designed to promote durable adhesion in the interphase region between the matrix and the embedded fibers. However, since strong adhesion minimizes interphase debonding during fiber fracture and increases a composite's strength, the energy released during fiber fracture creates matrix-cracks perpendicular to the length of the embedded fibers. Research suggests that these matrix-cracks promote catastrophic failure in composite lamina, thereby reducing the toughness of the composite.[3–5]

Therefore, interphase research is driven by the need to improve a composite's toughness while also improving its strength (longitudinal and transverse). In principle, one can control the IFSS and other interphase properties by proper fiber selection, fiber surface modification, and proper selection of the matrix resin. Therefore, it is also very important to evaluate exactly the IFSS thus controlled. For the last few decades, several techniques, such as the pull-out,[6–8] microbond,[9–13] fragmentation[14–20] and indentation[21] test methods, have been developed to achieve this goal.

Of the above techniques, only the fragmentation test loads the fiber in a manner consistent with composite loading. Until 1989, the fragmentation test had two major shortcomings: (1) the time required to test a single sample (∼ 5 h in the NIST laboratory) and (2) the inability of this test to assess the interac-

tion between closely space fibers as found in full composites. This year, Wagner and Steenbakker[21] developed a methodology for preparing 2-D closely spaced multi-fiber test specimens to assess micro-damage in fibrous composites. This approach admits the systematic study of how the micromechanics of stress transfer and composite failure modes are influenced by micromechanics and microstructural properties. The critical properties that can be investigated by this technique are chemical modification of the fiber/matrix interfacial layer, matrix modification, fiber–fiber interactions (fiber bunching), fiber misalignment or slack, fiber configuration in hybrid composites, and failure dynamics (crack speed variations). In addition, this approach has the potential to assess how the above properties influence failure parameters (e.g., the critical crack size, k^*, or the correlation length δ) that are used in composite statistical failure models.[22]

Recent investigations[23–31] using the Wagner/Steenbakkers approach have focused on carbon fibers, aramid, or Nicalon silicon carbide fibers embedded in diglycidyl ether of bisphenol-A (DGEBA) and/or polyglycol diepoxide resins cured with flexible curing agents (e.g., poly(oxypropylene) triamine and tetraethylene pentamine). The major driving force for using carbon fibers and aramid fibers is the use of Laser Raman spectroscopy (LRS) to detect the stress in the embedded fibers.

Although the results from these analyses are applicable in principle to glass fiber, which is not amenable to LRS, the IFSS and interphase region can be modified to a much greater extent using silane cross coupling (SCC) technology. In addition, the matrix material in structural composites is more brittle and has a higher glass transition temperature. Results by Drzal's research group[4] have shown that the use of SCC technology on glass fibers changes the failure mode of the interphase region during fiber fracture from debonding only (bare E-glass (water-sized) fibers) to debonding with matrix crack formation (E-glass fibers treated with an epoxy compatible size). Interestingly, the IFSS between the two systems are comparable. In addition, the changes in micromechanics failure behavior correlated with changes in macroscopic failure behavior. Unidirectional composites composed of water-sized fibers failed in a ductile like manner, while unidirectional composites made with the treated fibers failed in a brittle manner. Since 90% of all composites are composed of glass, a research program was initiated at NIST to systematically investigate how the critical properties mentioned above influence failure initiation and propagation in glass composites.

The authors[14] reported in a previous paper, in the case of interfiber spacing being too close in the multiple glass fiber fragmentation test, one fiber breaks,

causing the other fiber to break. So, interfacial shear strength might be overestimated; but in the case that interfiber spacing was large enough, there was no fiber-fiber interaction. However, the authors[32] also reported recently that interfacial shear strength decreased with the decreasing interfiber distance using two-dimensionally glass fiber arranged fragmentation test sample.

The objective of this article is to gain a fundamental understanding of the interplay between fiber breaks in case of the interfiber distance is too close and large enough using two fiber model composites.

In this article, the effect of interfiber distance on the interfacial properties in E-glass fiber/epoxy resin composites has been investigated using one and two fiber with various interfiber distance fragmentation test specimens. In addition, the effect of water-sized E-glass fibers and E-glass fibers coated with an epoxy compatible industrial sizing of known composition on the interfacial properties has been studied.

EXPERIMENTAL

Materials

OSi Specialties-Crompton Corporation[*] coated the E-glass fibers from an aqueous solution consisting of 5 g of γ-aminopropyl triethoxysilane dissolved in 995 g of distilled water. The solution was adjusted to pH 4 using glacial acetic acid. These fibers and the water-sized (bare) E-glass fibers, also obtained from OSi Specialties, were used as received. The water-sized fibers were washed with distilled water and dried at 80°C for 72 h. Hence the fibers contained no processing aids or coupling agents to promote adhesion.

The diglycidyl ether of bisphenol-A (DGEBA, Epon 828, Shell) was used as the matrix resin. The resin was cured with a stoichiometric amount (14.5 g per 100 g of resin) of *meta*-phenylene diamine (*m*-PDA, Fluka Chemical), and the ultimate tensile strain of the resin was 7.8%.

Single fiber tensile test

The tensile strength was measured on single fibers using a United Model FM-10 tensile tester equipped with a 100 g load cell. The specimens had a gauge length of 20 mm and the specimens were tested at a crosshead speed of 2.0 mm/min. Before testing, the

---

[1]Certain commercial materials and equipment are identified in this article in order to specify adequately the experimental procedure. In no case does such identification imply recommendation or endorsement by the National Institute of Standards and Technology, nor does it imply necessarily that the items are the best available for the purpose.

diameter of every sample was measured with an optical micrometer (VIA-100, Boeckeler).

Preparation of fragmentation test samples

The sample preparation for single- and two-fiber test specimens were similar to that described by Drzal et al.,[14] and a brief description follows. The silicone (GE silicone RTV-664) mold with eight dog-bone-shaped cavities was used for the preparation of fragmentation test samples. Each cavity in the mold has 400-μm-wide sprue slots in the center of each cavity end to aid in aligning the fiber in the center of the cavity. Single fibers were aligned in the sprue slots by hand. Two fiber specimens were placed in each cavity using the device. This device utilizes the fiber-positioning concept outlined by Wagner and Steenbakker[21] to alter the spacing between the fibers. However, the device was modified to admit placement of the fibers into the dog bone shaped cavities of the RTV-664 mold. A detail description of this apparatus is in preparation. In each case, the fiber ends were fixed in place by putting a small drop of five-minute epoxy resin (Hardman Adhesives) at the far end of each sprue slot.

The single- and two-fiber specimens were prepared with DGEBA epoxy resin cured using *m*-PDA. One hundred grams of DGEBA and 14.5 g of *m*-PDA were weighed out in separate beakers. To lower the viscosity of the resin and melt the *m*-PDA crystals, both beakers were placed in separate vacuum ovens (Fisher Scientific Isotemp Vacuum Oven, model 281 A) set at 65°C. After the *m*-PDA crystals were completely melted, the silicone rubber molds containing the fibers were placed into another vacuum oven (Fisher Scientific Isotemp Vacuum Oven, model 281 B) that was preheated to 75°C at −20 KPa, for 20 min. This last procedure dries the molds and minimizes the formation of air bubbles during the curing process. At ∼ 9 min before the preheated molds were removed from the oven, the *m*-PDA is poured into the DGEBA and mixed thoroughly. The mixture was placed into the vacuum oven and degassed for ∼ 7 min. After 20 min, the preheated molds were removed from the oven and filled with the DGEBA/*m*-PDA resin mixture using 10 mL disposable syringes. The filled molds were then placed into a programmable oven (Blue M, General Signal, model MP-256-1, GOP). A cure cycle of 2 h at 75°C followed by 2 h of post curing at 125°C was used.

Fragmentation test

Fragmentation tests were carried out on an automated fragmentation test machine (Gaithersberg, MD). Sheldon Wesson, formerly at Textile Research Institute, built this machine to NIST specifications. A detailed description of this machine is in preparation.

Before testing, samples were polished by emery paper of Nos. 800 and 2400 to remove stress concentration sites at the edge part of the sample. To facilitate strain measurements, transverse fiducial marks (∼ 10 mm apart) were applied to each end of the specimen gauge length by a blue color permanent pen. Strains at each step were calculated using the scanned images of each step. The total strain in the sample at the end of the test was about 6.0%.

Specimen slippage during testing was minimized by installing the specimen in the grips with moderate tightness. The specimen was then loaded in tension by the sequential application of step-strains. During the test, twenty-eight step-strains were applied and total deformation was ∼ 2.4 mm. Each step-strain was applied at a rate of 85 μm/s and the average deformation in the specimen during each step-strain was 85.7 μm. The delay time between the applications of successive step-strains was 10 min. The image was scanned before and after every step-strain using a movable camera. The digital image was saved automatically on the computer. The scanning length was 23 mm. After 28 steps, the sample was unstressed and removed.

The tested specimen was then mounted on the manual fiber fragmentation testing machine (manual
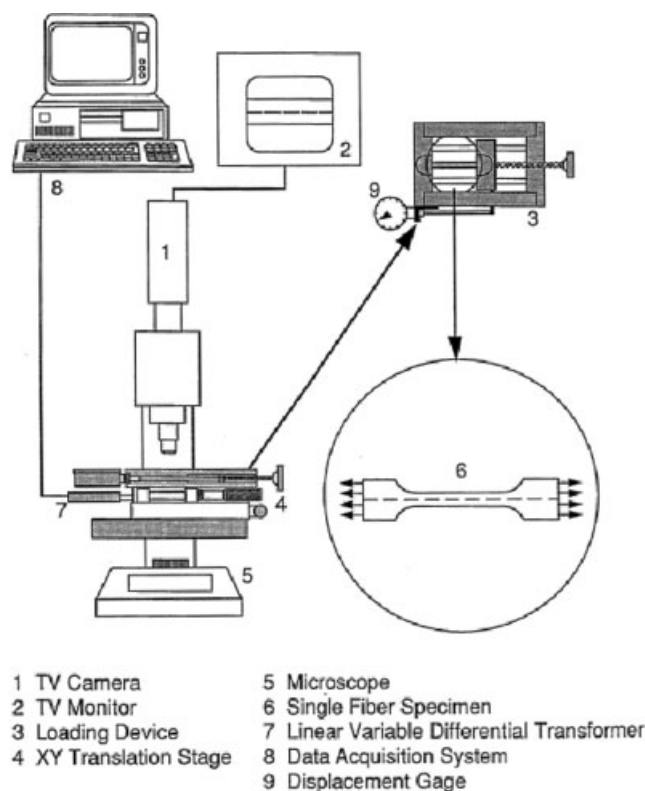

1 TV Camera	5 Microscope
2 TV Monitor	6 Single Fiber Specimen
3 Loading Device	7 Linear Variable Differential Transformer
4 XY Translation Stage	8 Data Acquisition System
	9 Displacement Gage

Figure 1 Schematic of manual fiber fragmentation test machine.

TABLE I
Tensile Strength of Single Fiber E-Glass Specimens

Fiber treatment	Sized fiber	Unsized fiber
Tensile strength, GPa	2.10 ± 0.57	1.63 ± 0.44
Shape parameter, α	3.998	3.993
Scale parameter, β	2.266	1.820

FFTM) to measure fragment lengths and photograph birefringence enhanced images of the fiber breaks (Fig. 1). The procedure for measuring fragments has been described previously.[33] The images were obtained by installing a CCD camera (Optronics LX-450 RGB Remote-Head microscopic camera) on the manual FFTM.

Interfacial shear strength calculations

The interfacial shear strength was calculated using the Drzal variant[14] of the Kelly-Tyson formulism, where the matrix is assumed to conform to the elastic-perfectly plastic constitutive law. In the original formulation [eq. (1)], the fiber diameter (D_f), critical transfer length (l_c), and fiber strength at the critical transfer length (σ_f) are used to calculate the interfacial shear strength. Typically, l_c is estimated from the average length of the fragments at saturation, i.e., the point where no additional fragments fracture with increasing strain. Drzal advocates obtaining Weibull type parameters (α and β) by using the two-parameter Weibull model to fit a plot of the failure probability relative to the fiber fragment length at saturation. The distribution of fiber fragment lengths have been satisfactorily described by a two parameter Weibull analysis (Figs. 3 and 4). Therefore, following eq. (2) is used in this article to determine the interfacial shear strength.[14]
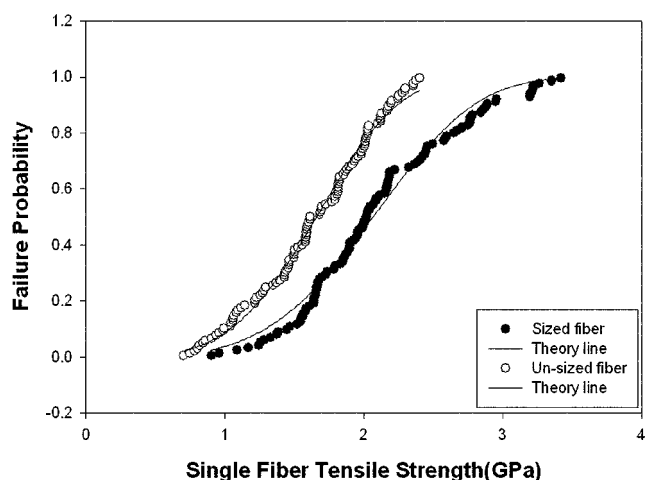

Figure 3 Failure probability versus fiber fragment aspect ratio for sized E-glass fibers tested by the single fiber fragmentation test. The data are fit to the 2-parameter Weibull probability distribution function.

$$\tau = \frac{\sigma_f D_f}{2l_c} \tag{1}$$

$$\tau = \frac{\sigma_f}{2\beta}\Gamma\left(1 - \frac{1}{\alpha}\right) \tag{2}$$

In the eq. (2), α and β are the shape and scale parameter, respectively, and Γ is the Gamma function. To eliminate contributions to σ_f that may arise from changes in the interfiber spacing, σ_f was estimated from the single fiber tensile test using 20 mm of gauge length specimens. A recent review of single fiber test methodologies by Holmes[34] compares this analysis approach to other analysis methods that have been used to determine the interfacial shear strength.

Figure 2 Failure probability plots of sized and unsized single fiber strength distributions for 20 mm gauge lengths. The data are fit to the 2-parameter Weibull probability distribution function.
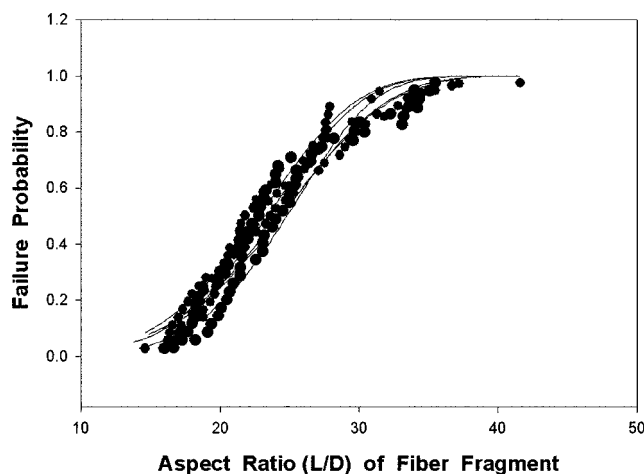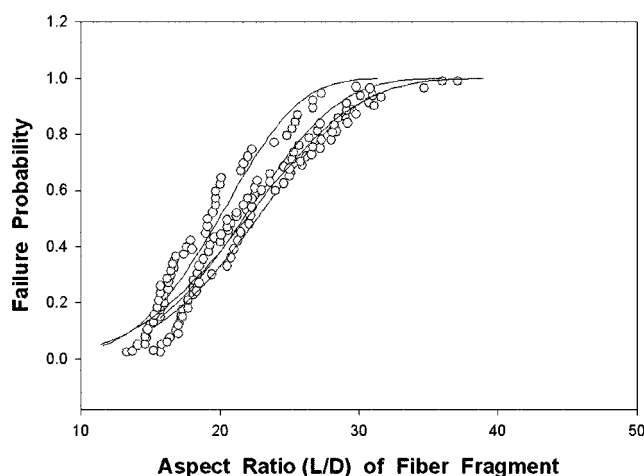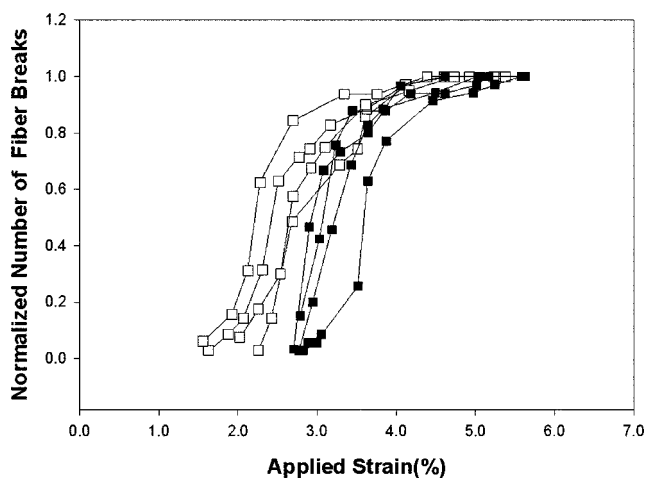

Figure 4 Failure probability versus fiber fragment aspect ratio for unsized E-glass fibers tested by the single-fiber fragmentation test. The data are fit to the 2-parameter Weibull probability distribution function.

Figure 5 Plots of normalized number of fiber breaks as a function of applied strain for E-glass fiber/DGEBA/ *m*-PDA single-fiber fragmentation test specimens. The solid squares represent data from sized fibers and the open squares represent data from unsized fibers.

RESULTS AND DISCUSSION

Single fiber tensile test

In Table I, the tensile strengths of sized and unsized E-glass single fibers are given. Since it is known that sizing protects glass fibers from damage during processing operations, the higher tensile strength of the sized fiber is expected. Figure 2 shows the relationship between failure probability and single fiber tensile strength. Solid lines, obtained by the Weibull distribution function with two parameters, exhibit an excellent fit to the experimental data.

Single-fiber fragmentation test

Figures 3 and 4 represent plots of failure probability as a function of fiber fragment aspect ratio for data obtained from the single fiber fragmentation test. Solid line plots, obtained from the 2-parameter Weibull distribution function, fit these data. For the sized fibers shown in Figure 3, the aspect ratio ranges from 15 to 37, while the unsized fibers shown in Figure 4 ranges from 12 to 33.

Figure 5 represents the normalized number of fiber breaks as a function of applied strain from the data obtained from the SFFT of the sized and unsized test specimens. Consistent with the lower fiber strength obtained from the single fiber tensile tests above, the initial fiber breaks in the unsized

TABLE II
Interfacial Shear Strength of E-Glass Fiber/Epoxy Resin

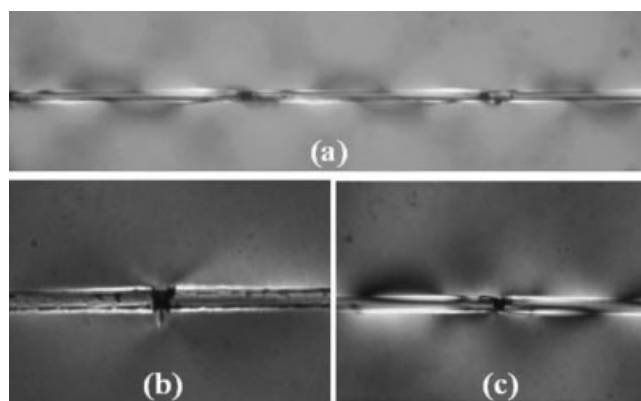| Fiber treatment	Sized fiber	Unsized fiber
Interfacial shear strength, MPa	46.70 ± 2.59	40.69 ± 2.60

Figure 6 Polarized transmitted light micrographs of the sized E-glass fiber/epoxy resin fragmentation test (a) at saturation, (b) fiber break with matrix crack, (c) fiber break with debonding only.

test specimens occurred at a lower strain value ($\approx$ 2%) than the sized fiber test specimens ($\approx$ 3%). As a result, saturation in the un-sized test specimens was achieved at a lower strain value than the sized specimens. Using these data and the fiber strengths determined from single fiber tensile tests, the interfacial shear strength of the sized fiber test specimens were on average only 15% higher than the unsized fiber specimens (Table II).

Consistent with these results, polarized transmitted light micrographs of the sized and unsized E-glass fibers at saturation were found to be similar (compare Figs. 6 and 7). Although some fiber breaks in the sized test specimens occurred with debonding only [Fig. 6(c)], fiber breaks were most often accompanied by debonding with matrix crack formation [Fig. 6(b)]. In contrast, fiber breaks in the unsized fiber specimens occurred with debonding only [Fig. 7(b)]. In the unsized specimens, the only fiber breaks with matrix cracks were associated with fiber breaks that occurred during the curing of the speci-
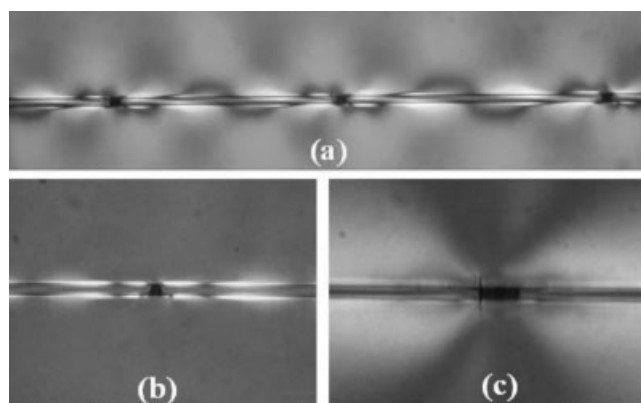

Figure 7 Polarized transmitted light micrographs of the un-sized E-glass fiber/epoxy resin fragmentation test (a) at saturation, (b) fiber break with debonding only, and (c) fiber break with matrix crack.
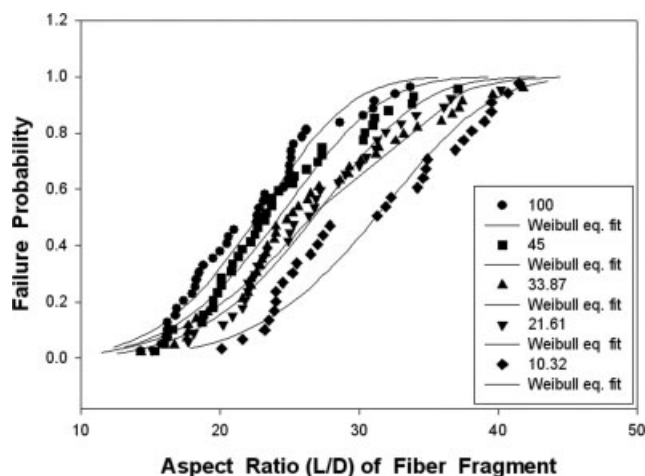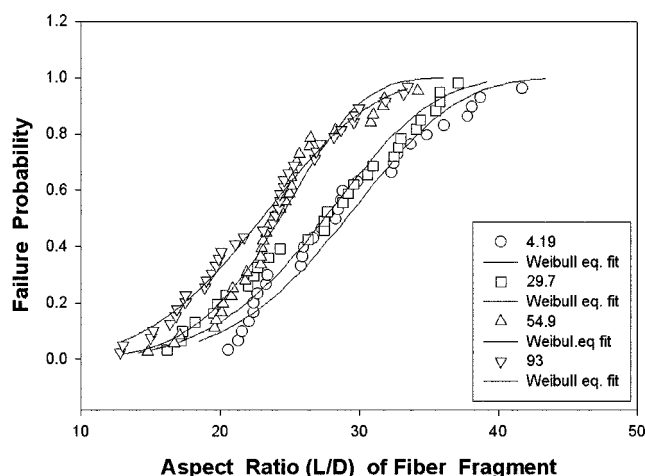
Figure 8 Plots of failure probability versus fiber fragment aspect ratio and interfiber distance for sized E-glass fibers tested by the two-fiber fragmentation test. The data are fit to the 2-parameter Weibull probability distribution function. The numbers show an interfiber distances (μm).

men [Fig. 7(c)]. These results are consistent with similar results obtained by Drzal et al.[4] for epoxy-sized and unsized E-glass fibers embedded in a DER 383 DGEBA epoxy resin cured with 1,2-diaminocyclohexane curing agent. Drzal suggested that differences in the macroscopic failure behavior of unidirectional sized and unsized E-glass fiber laminates when deformed in flexure were associated with failure behavior differences observed in the single fiber fragmentation tests.

Two-fiber fragmentation test

Figures 8 and 9 show plots of the failure probability as a function of aspect ratio and interfiber distance

for the sized and unsized two-fiber fragmentation test specimens. As before, the solid lines are plotted from the two-parameter Weibull distribution function. In both cases, the probability curve shifts to longer aspect ratios with decreasing interfiber distance. In statistics failure models, this would correspond to a change in the correlation length δ with interfiber distance.[22]

Although the two sets of curves overlap at interfiber distances greater than 30 μm (2 fiber diameters), comparing the location of the 4 μm interfiber spacing curve for the unsized fibers with the 10 μm interfiber curve for the sized fibers indicates a significant increase in the average fragment length size of the sized fiber specimens and suggests a more pronounced interaction between the two sized fibers with an interfiber spacing of less than 2 fiber diameters.

In Figures 10 and 11 plot of the normalized number of fiber breaks as a function of applied strain and interfiber distance for the sized and unsized, respectively, E-glass fiber/DGEBA/m-PDA two-fiber fragmentation test specimens are shown in Figures 10 and 11, respectively. In Figure 10, initial fiber breaks in the two-fiber sized specimens occur at ~ 3% strain, while those for the two-fiber unsized specimens (Fig. 11) occur between strains of 2 to 2.5%. These results are consistent with the initial fiber breaks as they occur in the single-fiber test specimens (Fig. 5). From the data the interfiber spacing does not appear to influence the strain where the initial fiber break occurs. However, below 50 μm interfiber spacing does influence the interfacial shear strength as determined from the two-fiber fragment length data at saturation (Fig. 12). Above 50 μm, the interfacial shear strength from the two-fiber frag-

Figure 9 Plots of failure probability versus fiber fragment aspect ratio and interfiber distance for un-sized E-glass fibers tested by the two-fiber fragmentation test. The data are fit to the 2-parameter Weibull probability distribution function. The numbers show interfiber distances (μm).
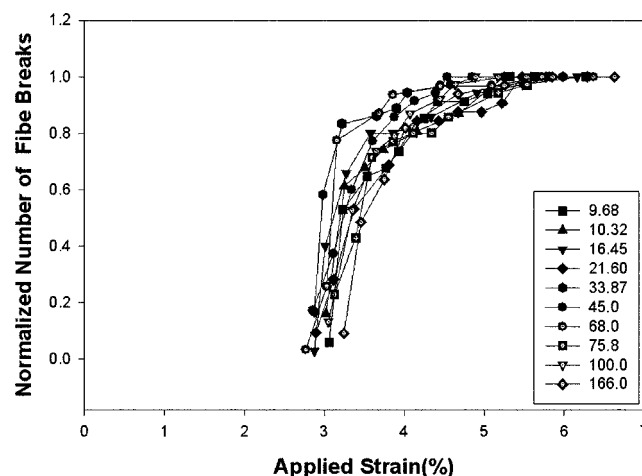

Figure 10 Plots of normalized number of fiber breaks as a function of applied strain and interfiber spacing for sized E-glass fiber/DGEBA/m-PDA two-fiber fragmentation test specimens. The numbers show interfiber distances (μm).
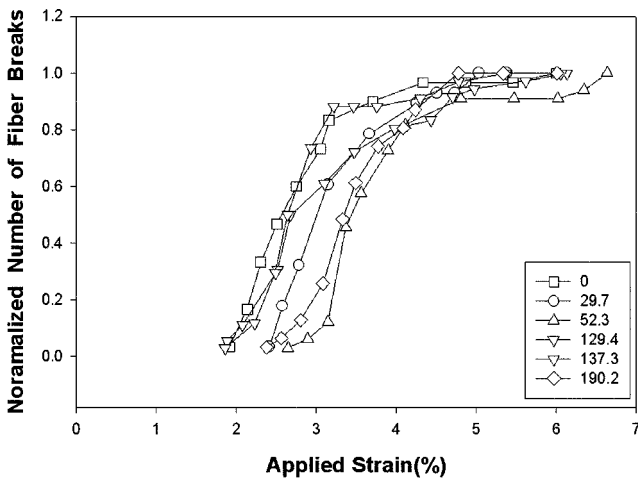
Figure 11 Plots of normalized number of fiber breaks as a function of applied strain and interfiber spacing for unsized E-glass fiber/DGEBA/*m*-PDA two-fiber fragmentation test specimens. The numbers show an interfiber distances (μm).

ment test is constant and consistent with results from the single-fiber fragmentation test.

In the other words, in case of the interfiber distance of under 50 μm, the interfacial shear strength decreased with decreasing the interfiber distance and the extent of the decreasing was more serious as the increasing of the number of adjacent fiber. This is probably that the interface between the fiber and the resin was damaged by the adjacent fiber breaks and the damage increased with closing the interfiber spacing and the number of adjacent fiber. We can guess from this interfacial shear strength in real composites is much smaller than that of multifiber fragmentation sample with touched fiber.

It was seen that the interfacial shear strengths saturated when the interfiber distance was over 50 μm, the ones were saturated regardless of fiber surface
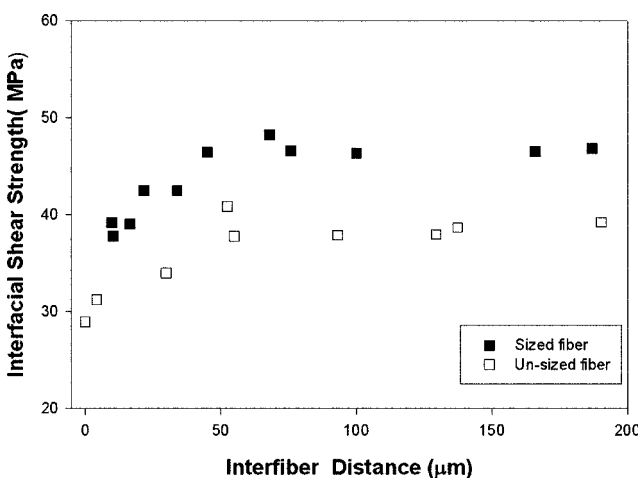

Figure 12 Interfacial shear strength versus interfiber distance as determined from two-fiber fragmentation test.
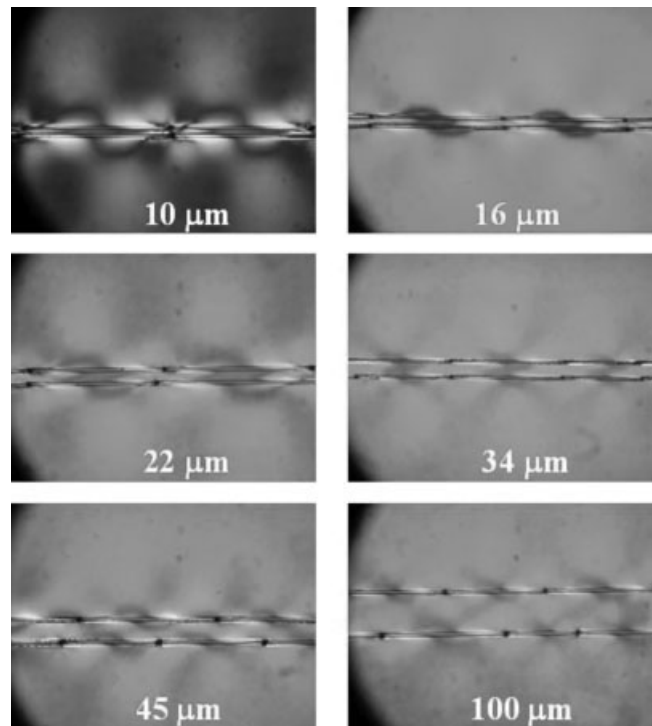

Figure 13 Collage of polarized transmitted light micrographs of sized two fibers E-glass/DGEBA/*m*-PDA fragmentation test specimens as a function of interfiber distance at saturation.

treatment and the ones were in close agreement with those of the single fiber fragmentation test.

The damaging factors considered owing to fibers break and debonding are strain energy release, stress transfer and stress concentration, etc.[35] The extent of stress concentration depends on mainly exiting matrix crack in case of sized fiber sample. Therefore, it was shown that when the interfiber distance is small, the decreasing of interfacial shear strength in sized fiber fragmentation was more serious than the decreasing of the one in the desized fiber fragmentation test.

To better understand how fiber–fiber interactions influence interfacial shear strength, collages of the polarized transmitted light micrographs as a function of interfiber distance for the sized and unsized two-fiber fragmentation specimens are shown in Figures 13 and 14, respectively. In both cases, the birefringence patterns in the matrix of closely-spaced fibers overlap extensively in the region between the fibers yielding a combined birefringence pattern suggestive of a single fiber. As the interfiber spacing increases the intensity of this interaction decreases, yielding independent separate birefringence patterns for each fiber. Consistent with these observations, the location of fiber breaks between fibers goes from coordinated to random as the interfiber spacing increases.

A close examination of the data from the two-fiber sized specimens suggests that this shift from coordinate to random fracture sites between fibers corre-
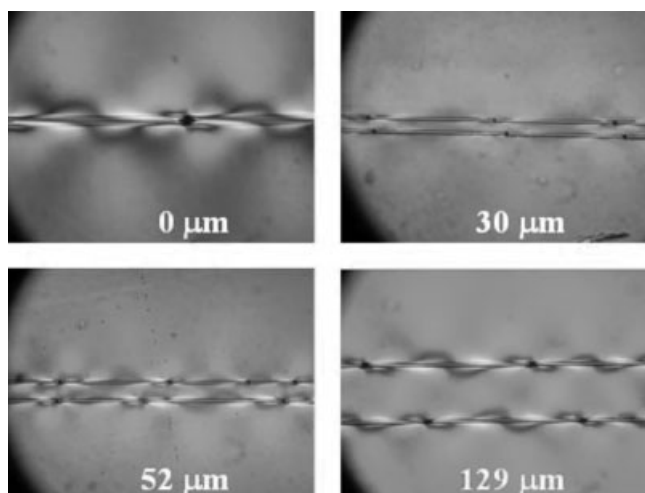
Figure 14 Collage of polarized transmitted light micrographs of unsized two fiber E-glass/DGEBA/*m*-PDA fragmentation test specimens as a function of interfiber distance at saturation.
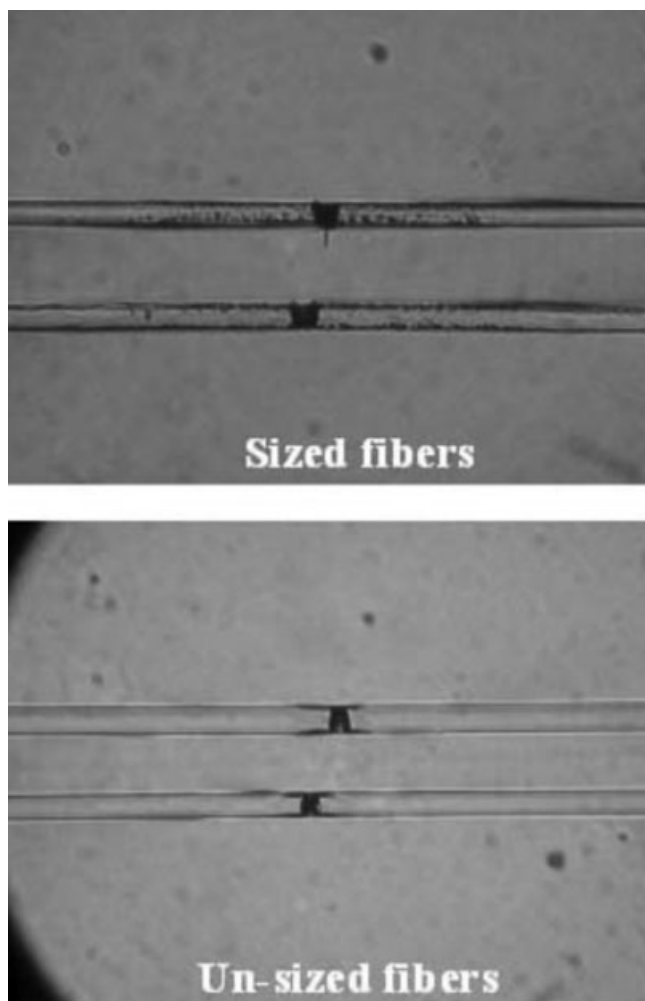

Figure 15 Micrographs comparing fiber-fiber interaction in sized and unsized E-glass/DGEBA/*m*-PDA fragmentation test specimens.

lates with interfiber spacing up to ∼ 50 μm. When 40 breaks in each test specimen were analyzed, all the breaks were coordinated when the interfiber distance is 10 μm or less. From interfiber spacing of 16 to 22 μm all but one set of breaks were coordinated. At an interfiber spacing of 34 μm, six sets of breaks were found to be random. Above 45 μm, all the break positions were independent of the adjacent fiber crack location.

Figure 15 shows coordinated pairs of breaks from sized and unsized fragmentation specimens. The damage induced by the matrix crack on the adjacent fiber is greater in the sized specimen (observe roughness around fiber break) than in the unsized fiber. This occurs despite the closer spacing between fibers in the un-sized specimen (2 versus 3 fiber diameters). Additional evidence of damage induced by matrix cracks can be found in the collage shown in Figure 16.

In subparts (a) and (b) of this collage, the fiber break appears to penetrate through the touching adjacent fibers. Based on our analysis of the fractured surfaces of test specimens that broke during testing, this is an optical effect caused by the directional nature of the penny shaped matrix crack (Figs. 4 and 5 of Ref. 36). However, it should be noted that fracturing of closely spaced adjacent fibers has been observed in the NIST laboratory for E-glass fibers
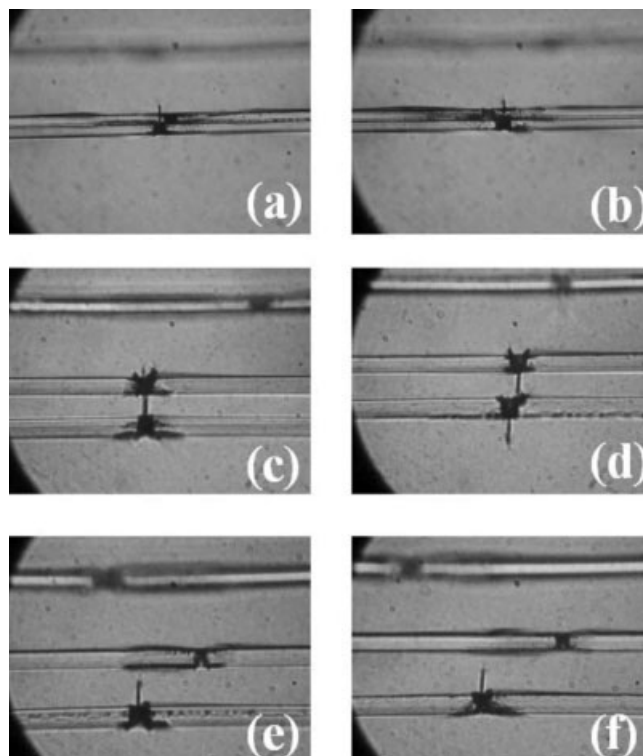

Figure 16 Collage of micrographs showing interactions between fiber breaks in sized E-glass/DGEBA/*m*-PDA fragmentation test specimens.

coated with a similar sizing. The damage observed in the touching fibers has also been observed in touching unsized E-glass/DGEBA/*m*-PDA systems. However, the damage induced on the adjacent fibers by the matrix cracks shown in subparts (e) and (f) of this collage have not been observed in nontouching unsized E-glass/DGEBA/*m*-PDA systems of comparable interfiber spacing.

At present, it is assumed that the ±45° shear bands emanating from the tips of the matrix crack in tension influence the stress state in the adjacent fiber and its surrounding matrix.[36] Initial finite element analysis (FEA) results (not shown) suggests that the most intense interaction between the shear bands emanating from the matrix crack shown in Figure 16(e) and the adjacent fiber occurs at a distance of ∼ 15 μm. In micrographs (e) and (f), the tips of the matrix crack are clearly within 1 fiber diameter (15 μm) of the adjacent fiber. The exact manner in which these shear bands perturb the stresses in the adjacent fiber and cause damage to the matrix surrounding the adjacent fiber is still under investigation.

CONCLUSIONS

The effect of interfiber distance and fiber surface treatment on the interfacial properties in E-glass fiber/epoxy resin composites has been studied and the findings made from this study can be summarized as follows.

1. Consistent with the results published by the Drzal group,[4] the interfacial shear strength of bare E-glass fibers was found to be lower than observed for E-glass fibers coated with an epoxy-compatible size. In addition, during fiber fracture, the bare E-glass fibers failed by fiber-matrix debonding only, while the sized fiber failed by debonding with matrix crack formation.

2. Data from multi-fiber tests revealed a coordinated fracture pattern when the interfiber distance was below 50 μm. Above 50 μm, the crack positions in adjacent fibers were random (i.e., independent of adjacent fiber crack location).

3. Consistent with these results, the stress distribution pattern in the multi-fiber saturated test specimens mimicked those of a single fiber at very close interfiber spacing. The stress distributions of adjacent fibers were decoupled above an interfiber distance of 50 μm.

4. Between (0 and 50) μm, the interfacial shear strength increased with increasing interfiber distance. Above 50 μm, the interfacial shear strengths of fibers in multifiber test specimens were constant and consistent with those from the single fiber fragmentation test.

5. At comparable interfiber distances, collateral damage to adjacent fibers arising from fiber fracture appeared to be more pronounced in sized fibers that fracture with matrix crack formation.

References

1. Hancock, P.; Cuthbertson, R. C. J Mater Sci 1970, 5, 762.
2. Spanoudakis, J.; Young, R. J. J Mater Sci 1984, 19, 487.
3. Agarwal, B. D.; Broutman, L. J. Analysis and Performance of Fiber Composites, 2nd ed.; Wiley: New York, 1990; p 87.
4. Drown, E. K.; Al Moussawi, H.; Drzal, L. T. J Adhes Sci Technol 1991, 5, 865.
5. DiLandro, L.; Pegoraro, M. J Mater Sci 1987, 22, 1980.
6. Takali, A.; Arridge, R. G. C. J Phys D: Appl Phys 1973, 6, 2038.
7. Bowling, J.; Groves, G. W. J Mater Sci 1979, 14, 431.
8. Penn, L. S.; Lee, S. M. Fiber Sci Technol 1982, 17, 91.
9. Miller, B.; Muri, P.; Rebenfeld, L. Compos Sci Technol 1987, 28, 17.
10. Gaur, U.; Miller, B. Compos Sci Technol 1989, 34, 35.
11. Moon, C. K.; Cho, H. H.; Lee, J. O.; Park, T. W. J Appl Polym Sci 1992, 44, 561.
12. Moon, C. K.; Lee, J. O.; Cho, H. H.; Kim, K. S. J Appl Polym Sci 1992, 45, 443.
13. Moon, C. K. J Appl Polym Sci 1994, 54, 73.
14. Moon, C. K.; Mcdonough, W. G. J Appl Polym Sci 1998, 67, 1701.
15. Drzal, L. T.; Rich, M. J.; LLoyd, P. F. J Adhes 1983, 16, 1.
16. Drzal, L. T. SAMPE J 2002, 19, 7.
17. Bascom, W. D.; Jensen, R. M. J Adhes 1986, 19, 219.
18. Curtin, W. A. J Mater Sci 1991, 26, 5239.
19. Waterbury, M. C.; Drzal, L. T. J Compos Technol Res 1991, 13, 22.
20. Baxevanakis, C.; Jeulin, D.; Valentin, D. Compos Sci Technol 1993, 48, 47.
21. Wagner, H. D.; Steenbakkers, L. W. J Mater Sci 1989, 24, 3956.
22. Smith, R. L.; Phoenix, S. L.; Greenfield, M. R.; Henstenburg, R. B.; Pitt, R. E. Proc R Soc London Ser A 1983, 388, 353.
23. van den Heuvel, P. W. J.; Peijs, T.; Young, R. J. J Mater Sci Lett 1996, 15, 1908.
24. van den Heuvel, P. W. J.; vanderBruggen, Y. J. W.; Peijs, T. Compos A 1996, 27, 855.
25. van den Heuvel, P. W. J.; Peijs, T.; Young, R. J. Compos Sci Technol 1997, 57, 899.
26. van den Heuvel, P. W. J.; Wubbolts, M. K.; Young, R. J.; Peijs, T. Compos A 1998, 29, 1121.
27. van den Heuvel, P. W. J.; Peijs, T.; Young, R. J. Compos Sci Technol 1998, 58, 933.
28. van den Heuvel, P. W. J.; Peijs, T.; Young, R. J. Compos A 2000, 31, 165.
29. Grubb, D. T.; Li, Z. F.; Phoenix, S. L. Compos Sci Technol 1995, 54, 237.
30. Li, Z. F.; Grubb, D. T.; Phoenix, S. L. Compos Sci Technol 1995, 54, 251.
31. Moon, C. K.; McDonough, W. G. Polymer 1995, 19, 835.
32. Moon, C. K.; Holmes, G. A.; McDonough, W. G. J Appl Polym Sci 2006, 99, 1541.
33. Holmes, G. A.; Peterson, R. C.; Hunston, D. L.; McDonough, W. G. Polym Compos 2000, 21, 450.
34. Holmes, G. A. Mater Sci Eng R-Rep, to appear.
35. Smith, B. L.; Thompson J. B.; Schaffer T. E.; Viani, M.; Frederick, N. A.; Kindt, J.; Belcher, A.; Stucky, G. D.; Morse, D. E.; Hansma, P. H. Nature 1999, 399, 761.
36. Holmes, G. A.; McDonough, W. G. In Proceedings of the 47th International SAMPE Symposium and Exhibition—Science of the Advance Materials and Process Engineering Series, Long Beach, CA, 2002; p 1690.
37. Holmes, G. A.; McDonough, W. G.; Dunkers, J. P.; Han, C. C. J Polym Sci Part B: Polym Phys 2003, 41, 2976.